Li, Gen; Sang, Yushuai; Li, Xiang; Chen, Hong; Li, Yongdan

Solvolysis of enzymatic hydrolysis lignin in fuel compatible solvents

Published in:
Chemical Engineering Science

DOI:
10.1016/j.ces.2025.121549

Published: 15/05/2025

Document Version
Publisher's PDF, also known as Version of record

Chemical Engineering Science 310 (2025) 121549

Contents lists available at ScienceDirect

Chemical Engineering Science

journal homepage: www.elsevier.com/locate/ces

Solvolysis of enzymatic hydrolysis lignin in fuel compatible solvents

Gen Li [a], Yushuai Sang [a], Xiang Li [a], Hong Chen [b], Yongdan Li [a,*]

[a] Department of Chemical and Metallurgical Engineering, School of Chemical Engineering, Aalto University, Kemistintie 1, Espoo, P.O. Box 16100, FI-00076, Finland
[b] School of Environmental Science and Engineering, Tianjin University, Tianjin 300072, China

ARTICLE INFO

Keywords:
Enzymatic hydrolysis lignin
Solvolysis
Fuel compatible solvents
Molecular dynamics simulation

ABSTRACT

Enzymatic hydrolysis lignin (EHL), a by-product of bioethanol production, is regarded as a promising feedstock to produce chemicals and fuels, but its utilization has been limited. The solvolysis of EHL has been explored intensively in recent years and has progressed rapidly, particularly with the application of fuel-compatible solvents. This work reports EHL solvolysis at 240 °C in five solvents, i.e., dioxane, ethanol, ethyl acetate, heptane and water. Dioxane achieves the highest liquefaction degree, while ethanol yields the most monomers. In contrast, water and heptane result in inefficient liquefaction and monomer production. Simulation reveals that van der Waals and electrostatic interactions between solvents and EHL play different roles in dissolution process. Hydrogen bonds formed between the solvent and EHL facilitate the cleavage of the β-O-4 bonds, and hydrogen atom in the alkyl side chains tends to detach to form hydrogen radical, resulting in a self-supply of hydrogen atom.

1. Introduction

Lignocellulose, with cellulose, hemicellulose, and lignin as the three major components, is reproduced in huge amount every year by the biosphere and is one of the most important renewable resources critical to the carbon–neutral future chemical production (Li et al., 2015; Shen et al., 2022). The recently developed and growing second generation (2G) biofuel technology converts cellulose and hemicellulose in lignocellulose collected from agricultural and forestry residues into bioethanol as gasoline blend, but leaves lignin as a solid byproduct, known as enzymatic hydrolysis lignin (EHL). EHL has a large volume and contains a large ratio of the total energy of the original lignocellulose. Therefore, its value added utilization would add great economic output of the 2G biofuel process (Obydenkova et al., 2019). EHL as a kind of lignin, is rich in aromatic rings in its structure and its basic building blocks have been interpreted as syringic acid, coniferyl alcohol, p-coumaric acid, and ferulic acid, making it an ideal feedstock for the production of aromatic chemicals and commodity fuel blends (Fei et al., 2023; Li et al., 2015; Yang See et al., 2021). Furthermore, the properties of industrial EHL are also influenced by the type of biomass feedstock and the pretreatment processes applied. For instance, high-temperature pretreatments, such as steam explosion and dilute acid treatment, can induce lignin condensation, disrupt β-O-4 linkages, and consequently reduce its reactivity (Menezes et al., 2023).

Lignin solvolysis is a promising technology for obtaining lignin-derived chemicals and high-valued fuel molecules. Using fuel-compatible solvents allows dissolved lignin to be directly blended with conventional fuel, significantly enhancing the convenience and practicality of utilizing lignin-based biofuel. Additionally, solvents that produce toxic gases during combustion, such as those containing nitrogen or sulfur compounds, should be avoided to minimize environmental pollution. Several outstanding works have achieved complete liquefaction of lignin and high monomer yields (Barta et al., 2010; Huang et al., 2015a; Huang et al., 2014; Huang et al., 2015b; Nielsen et al., 2017; Yan et al., 2008). Barta et al. reported that under an Ar atmosphere at 300 °C, with $CuMgAlO_x$ as catalyst, lignin was converted to cyclohexyl derivatives in methanol without producing char and tar (Barta et al., 2010). Huang et al. employed the $CuMgAlO_x$ catalyst to depolymerize alkaline lignin in ethanol under an Ar atmosphere at 380 °C and obtained 60 wt% alkylated mono-aromatic compounds (Huang et al., 2015a; Huang et al., 2014; Huang et al., 2015b). In our previous works, various catalysts were used, including MoS_2 (Ma et al., 2023; Wu et al., 2023a), unsupported Ni (Sang et al., 2020; Sang et al., 2021), NiMo/Al_2O_3 (Bai et al., 2019), WO_3/Al_2O_3 (Mai et al., 2019), and α-MoC_{1-x}/AC (Ma et al., 2014) in ethanol or methanol, achieving complete liquefaction and high yield of alkyl phenols for 20–30 wt% at around 300 °C. In these reported works on catalytic lignin solvolysis, lignin is considered first dissolve and depolymerize in the solvent before contacting the

* Corresponding author.
E-mail address: yongdan.li@aalto.fi (Y. Li).

https://doi.org/10.1016/j.ces.2025.121549
Received 7 January 2025; Received in revised form 10 March 2025; Accepted 17 March 2025
Available online 19 March 2025

catalyst. However, due to its complexity and highly cross-linked structure, lignin cannot be effectively dissolved in most solvents at ambient temperature and these reported works were typically done in high temperature range, i.e., 200–380 °C to achieve complete lignin conversion and solvolysis.

Solvent is crucial for facilitating lignin solvolysis, as lignin dissolution and its macro molecular structure cleavage are necessary for the effective interaction with catalyst. In our recent works, we found that the van der Waals interactions between ethylene glycol and EHL could disrupt the π-π stacking in EHL, achieving complete solvolysis of EHL (Sang et al., 2023). In addition, a mixed solvent of water and isopropanol significantly improved the liquefaction degree of EHL, with 2 g of EHL being completely liquefied in 50 mL of solvent at 250 °C without forming char (Sang et al., 2024). Despite the intensive research already done on lignin solvolysis in various solvents, the underlying mechanisms for the dissolution and reaction steps remain unclear. Molecular dynamics (MD) simulation and density functional theory (DFT) calculation have been employed in investigating the microscopic mechanisms of lignin pyrolysis, e.g., MD simulation with reactive force fields (ReaxFF) (Chen et al., 2023; Pang et al., 2023; Ponnuchamy et al., 2021; Zhan et al., 2024; Zhang et al., 2019), DFT method to calculate the pyrolysis of lignin dimers and their cleavage steps (Fang et al., 2021; Jiang et al., 2019; Shen et al., 2021; Zhang et al., 2017). In addition, the force-field-based MD simulation was applied to investigate the self-assembly and dissolution of lignin in water, acetone, deep eutectic solvents, and ionic liquids (Sumer and Van Lehn, 2022; Wang et al., 2020; Wu et al., 2023b). Continuum solvation models, such as SMD-DFT, have also been utilized to estimate the solvation free energy of lignin fragments in aqueous and organic solvents, offering valuable thermodynamic insights into lignin-solvent interactions (Mariano Colombari et al., 2022).

In this work, the solvolysis of EHL was investigated using five different solvents: ethanol, ethyl acetate, dioxane, water, and heptane. Ethanol, ethyl acetate, dioxane, and heptane exhibit high compatibility with fuels, making them effective candidates for fuel blending. In addition, water, being the most abundant solvent on earth, was used as a reference for comparative analysis. The liquefaction degree of EHL and the yields of aromatic compound monomers were measured. With the MD technique, the average van der Waals interaction, electrostatic interaction, and the number of hydrogen bonds formed between the solvents and EHL were calculated. A slow growth (SG) sampling methodology was employed to examine the cleavage of the β-O-4 chemical bond and hydrogen transfer steps of a lignin dimer model compound. The new findings may provide a theoretical basis for the solvent selection for EHL solvolysis.

2. Experimental section

2.1. Materials

EHL, derived from corn cob biomass, was provided by Shandong Long Live biological technology Co (Sang et al., 2024)., Ltd. This type of EHL contains 91.2 wt% lignin, 1.42 wt% ash, and 0.12 wt% residual carbohydrate, and the weight percentages of C, O, H, N and S are 61.29, 29.61, 6.69, 0.98 and 0.01 wt%, respectively. The solvents (AR), including ethanol, ethyl acetate, dioxane, heptane, were all purchased from Sigma-Aldrich.

2.2. Depolymerization of EHL

Typically, 0.1 g EHL and 5 mL solvent were added in a 10 mL reactor. The loaded reactors were placed in a homogeneous reactor system (Kemi Co. Ltd, KMHR-8C) and heated at 240 °C for 5 h. Typically, each batch 5 reactors containing respectively one solvent was treated simultaneously. After the reaction the reactors were naturally cooled down to room temperature. The samples were filtrated to separate the solid and liquid products. The solid products were then dried in an oven at 70 °C for 12 h, followed by collection and weighing for further analysis.

2.3. Product analysis

The liquid product was qualitatively analyzed with a gas chromatograph-mass spectrometry (GC–MS, Agilent 6890-5973) and quantitatively analyzed with a gas chromatograph with a flame ionization detector (GC-FID, Agilent 6890). 3.33×10^{-4} g of anisole was added to the liquid products as the internal standard for quantification. The operating conditions of the GC part of GC–MS and GC-FID were identical. The column oven temperature was increased from 45 °C to 250 °C at a rate of 10 °C/min and held at 250 °C for 7 min. Both instruments used a weakly polar HP-5 MS capillary column (30 m × 0.25 mm × 0.25 μm) with a split ratio of 50. The mass spectrometer detector had no solvent delay, and the scan range was 10–500 *m/z*. The liquefaction degree and the monomer yield of EHL were calculated using equations (1) and (2), respectively (Sang et al., 2023):

$$\text{Liquefaction degree (wt \%)} = \left(1 - \frac{\text{The weight of the solid residue}}{\text{The weight of added EHL}}\right) \times 100\% \quad (1)$$

$$\text{Total yield of monomers (wt \%)} = \left(\frac{\text{The weight of total monomers}}{\text{The weight of added EHL}}\right) \times 100\% \quad (2)$$

2.4. Simulation methods

MD simulation was carried out using the Forcite module in Materials Studio 2018 software. The COMPASS II force field was employed to describe intermolecular interactions and assign charges (Shankar et al., 2022). Electrostatic interaction was described with the Ewald method with an accuracy of 0.001 kcal/mol, while van der Waals interactions were calculated with the atom-based method with a cutoff distance of 15.5 Å. The EHL polymer was constructed from 20 coniferyl alcohol (G) units of lignin. Five simulation boxes were established, each with dimensions of 60 × 60 × 60 Å, filled with one EHL polymer and enough solvent molecules. The solvent density was set to half of the real liquid solvent density at room temperature, consistent with experimental conditions, at 240 °C, 5 mL solvent in the 10 mL reactor completely vaporizes, and the average density of the system should be half of the liquid solvent's density. The canonical ensemble simulations (NVT) ensemble was used for MD simulation at 513 K for 2000 ps with a time step of 1 fs. The first 1000 ps was used for system equilibration, and the subsequent 1000 ps was used for data analysis. Nose-Hoover thermostat method was employed to control the temperature. The average interaction energies, i.e., the total interaction energy, van der Waals interaction energy, and electrostatic interaction energy, were calculated using the following formula:

$$\overline{E} = \frac{1}{n}\sum_{i=1}^{i=n}\left(E_{total}^{(i)} - E_{EHL}^{(i)} - E_{solvent}^{(i)}\right) \quad (3)$$

where E_{total}, E_{EHL}, and $E_{solvent}$ represent the energy of the system, lignin molecules, and the solvent, respectively. n is the total number of samples taken during data analysis.

All constrained ab initio molecular dynamics (cAIMD) simulation was carried out using the CP2K/Quickstep software package (VandeVondele et al., 2005). The electronic structure calculation employed the spin-polarized Perdew – Burke – Ernzerhof (PBE) functional combined with a double-zeta Gaussian basis set and plane wave (GPW) basis set, with an energy cutoff set to 600 Ry (Perdew et al., 1997). To accurately describe core electrons, the Goedecker – Teter – Hutter (GTH) pseudopotential was used, where the valence electron

counts for C, O, and H were 4, 6, and 1, respectively. cAIMD simulation was carried out with the NVT ensemble with a Nose − Hoover thermostat, a time step of 0.5 fs, and a target temperature of 240°C (Martyna et al., 1992). To accurately describe the non-covalent interaction, the DFT-D3 method proposed by Grimme et al. was employed in the simulation (Grimme et al., 2010). Phenoxyethylbenzene was used as the lignin dimer model compound to investigate the cleavage of the β-O-4 bond. Five simulation boxes were established, each with dimensions of 30 × 30 × 30 Å, filled with one phenoxyethylbenzene molecule and enough solvent molecules. The solvent density was set to half of the real liquid solvent density at room temperature, consistent with experimental conditions.

During the cAIMD simulation, the SG sampling method was used to simulate the β-O-4 bond cleavage and hydrogen transfer process in the lignin dimer model (Hu et al., 2002). The reaction coordinate was defined with the bond length of the β-O-4 bond as a collective variable (CV), with the rate of change of CV set to 0.0001 Å/step. The free energy change was calculated using thermodynamic integration, while the SHAKE algorithm was used to handle and maintain constraints within the molecules (Carter et al., 1989; Sprik and Ciccotti, 1998). The calculation formula is as follows:

$$\Delta A(\zeta_a, \zeta_b) = -\int_{\zeta_a}^{\zeta_b} F(\zeta)\, d\zeta \tag{4}$$

where $\Delta A(\zeta_a, \zeta_b)$ is the free energy difference between the two reaction coordinates ζ_a and ζ_b, and $F(\zeta)$ is the mean constraint force at the reaction coordinate ζ.

3. Results

3.1. Depolymerization of EHL

The solvolysis of 0.1 g EHL in 5 mL solvent was investigated at 240°C, see Fig. 1. EHL shows the best liquefaction performance in dioxane, with the liquefaction degree up to 94.6 wt%. Ethanol also exhibits a good liquefaction degree, 77.6 wt%. In contrast, ethyl acetate shows lower liquefaction degree of 59.7 wt%. The liquefaction degrees in water and heptane are both further lower, 41.9 and 23.3 wt%, respectively, and significant coking was observed with these two solvents. Thus, the order of liquefaction degree of EHL in different solvents is: dioxane > ethanol > ethyl acetate > water > heptane. For the monomer yield dioxane achieves 4.84 wt%, significantly lower than 6.54 wt% obtained with ethanol. The monomer yield in ethyl acetate is 5.15 wt%, slightly higher than that obtained in dioxane. The monomer yields are both very low in water and heptane, 2.57 and 1.34 wt%, respectively. Except for dioxane, the liquefaction degree and monomer yield in other solvents exhibit a similar order: ethanol > ethyl acetate > dioxane > water > heptane.

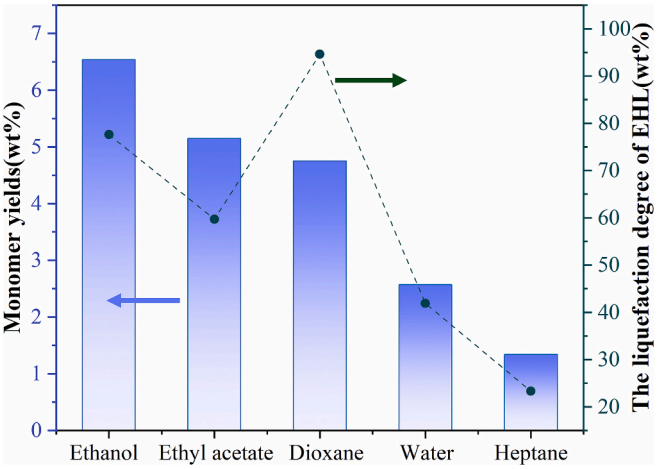

Fig. 1. Liquefaction degree and monomer yields of EHL solvolysis in different solvents.

Fig. 2(a)–(e) present the total ion chromatograms (TIC) of the liquid-phase products in various solvents. 17 monomer molecules were identified in the products. In ethanol, Fig. 2(a), the main monomers in the product included a significant amount of 4-vinylphenol and 2-methoxy-4-vinylphenol (4,6), which contain C=C double bond in side chain, as well as monomers with an aldehyde functional group in the side chain (9,10). In addition, ethyl p-coumarate (16) and ethyl ferulate (17) were also detected. Such esterss were not detected in the products obtained with other solvents, indicating that ethanol plays a role in stabilizing the radicals in EHL fragments by providing ethyl groups, leading to the formation of ester products (Huang et al., 2015b). In ethyl acetate and dioxane solvents, Fig. 2(b) and (c), the primary monomers were 4-vinylphenol (4) and 2-methoxy-4-vinylphenol (6) with C=C double bond in side chain, with fewer other monomers in products. With water, Fig. 2 (d), the main monomers in product were phenol, guaiacol, 2,6-dimethoxyphenol, 4-ethylphenol and 2-methoxy-4-ethylphenol (1,2,7,3,5), which have C-C single bonds. Monomers with C=C double bond in side chain were almost undetectable in the product. In heptane (Fig. 2(e)), the primary momoners were 2-methoxy-4-vinylphenol (6) with a C=C double bond in side chain, along with some 4-ethylphenol (3) and 2-methoxy-4-ethylphenol (5). Fig. 2(f) compares the content of four types of monomers obtained from EHL depolymerization in different solvents: 4-vinylphenol (4) and 2-methoxy-4-vinylphenol (6) with C=C double bonds, and 4-ethylphenol (3) and 2-methoxy-4-ethylphenol (5) with C-C single bonds. In water, the total content of these four monomers was the lowest, only 0.28 wt%, with almost no monomers containing C=C double bond in the product. In heptane, the total content of the four monomers was slightly higher than that in water, 0.87 wt%. In the other three solvents, the content of monomers with a C=C double bond in side chain was significantly higher than those with only C-C single bonds in side chain.

3.2. MD simulation of EHL liquefaction

Fig. 3(a)−(e) illustrate the stable states of EHL molecular chains in different solvents after 2000 ps simulation with NVT ensemble. The EHL is significant opened and stretched in dioxane, with the molecular structure appearing chain-like, corresponding to the best liquefaction performance, see Fig. 3(c). Although EHL also extends to some degree in ethanol, Fig. 3(a), the molecules do not fully stretch out, resulting in a lower liquefaction degree compared to that in dioxane. In contrast, the EHL molecular chains tend to aggregate in ethyl acetate, Fig. 3(b), water, Fig. 3(d), and heptane, Fig. 3(e), contributing to poor liquefaction performance of the solvents (Bogdan et al., 2023). This indicates that the stable states of EHL in different solvents obtained from MD simulations, are almost consistent with the order of liquefaction degree obtained in experiments.

Fig. 4(a) plots the interaction energies between solvents and the EHL model molecule. Ethanol, dioxane, and water have relatively high overall interaction energies with EHL, specifically −305.36, −330.93, and −313.02 kcal/mol, respectively. For dioxane, ethyl acetate, and heptane, the van der Waals interaction energy dominates, whereas in water, the electrostatic interaction energy is dominant. In ethanol, both van der Waals and electrostatic interaction energies contribute comparably. A linear fit of the data was performed to analyze the contributions of van der Waals and electrostatic interaction energies to the liquefaction degree of EHL. In Fig. 4(b), the data points are positioned close to the fitted plane, with a coefficient of determination (R^2) of 0.96, indicating an excellent correlation and high degree of fit. Fig. 4(c) illustrates the relationship between the predicted and actual liquefaction degrees, with data points closer to the Ideal Fit line indicating greater prediction accuracy. The fitted model function, as shown in Fig. 4(c), reveals that the coefficient for van der Waals interaction energy is 0.48, which is

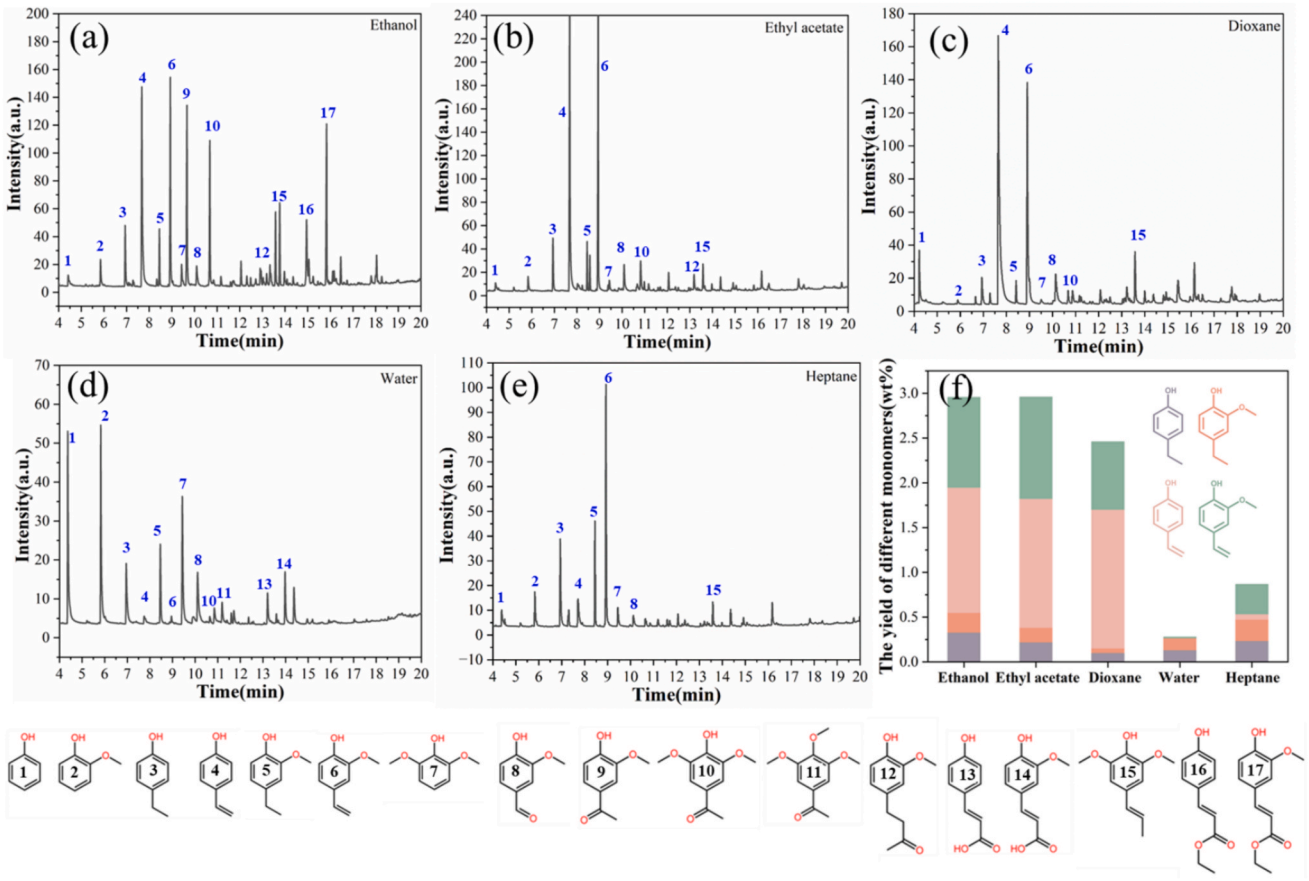

Fig. 2. (a–e) Total ion chromatograms (TIC) of dissolved EHL in the liquid phase and the structures of the aromatic monomer products, (f) content of four EHL monomers in different solvents.

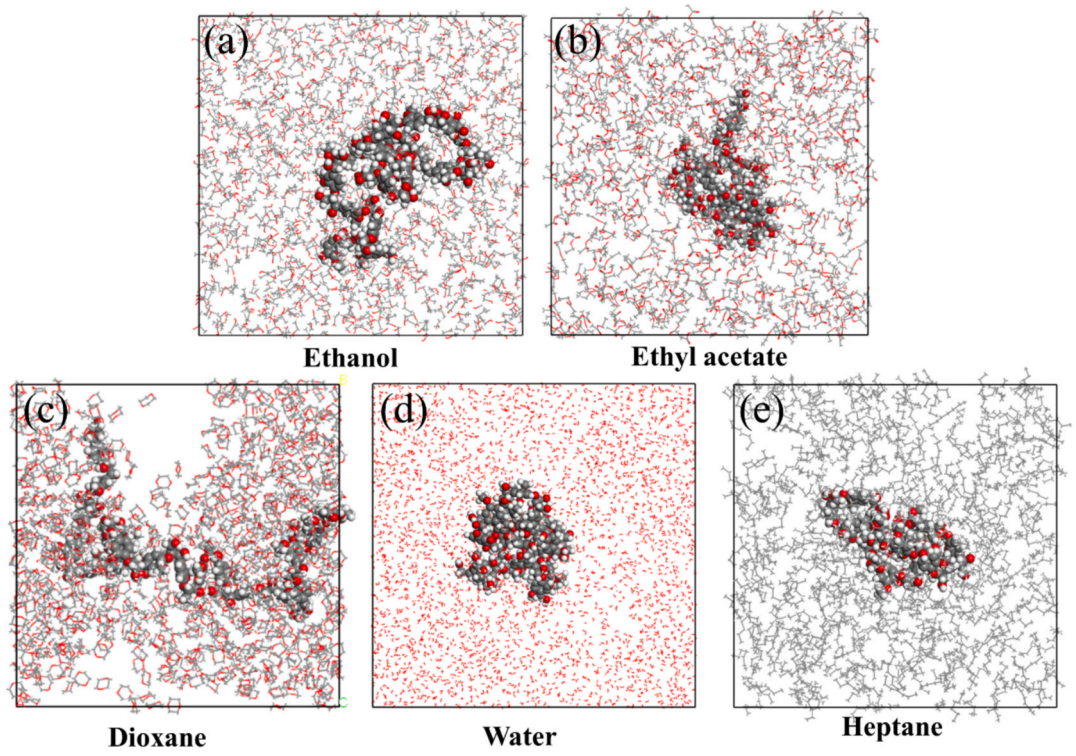

Fig. 3. Simulated models of EHL in different solvents.

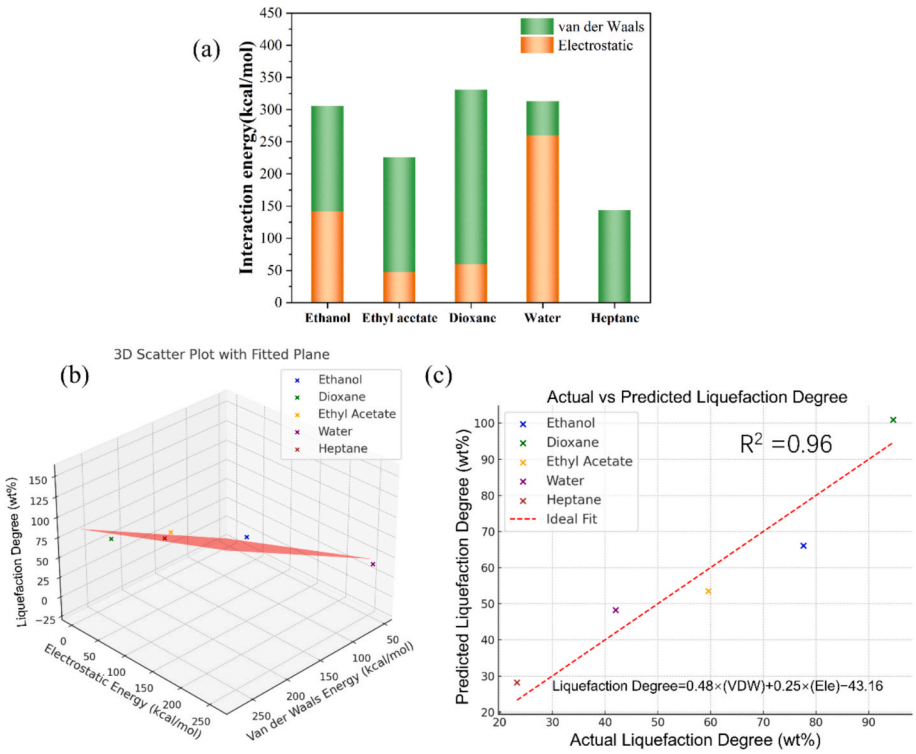

Fig. 4. (a) Average interaction energy between EHL molecules and different solvents, (b-c) the fitting relationship between van der Waals energy, electrostatic energy, and EHL liquefaction degree.

significantly higher than that of electrostatic interaction energy, which is 0.25. This is consistent with the findings of Hensen and his colleagues, who reported a linear correlation between the hydrogen bonding parameter (δ_H) of the solvents and the yield of solubilized lignin (Kouris et al., 2020). The results indicate that van der Waals forces have a more significant impact on the liquefaction degree of EHL compared to electrostatic forces. This also explains why water, ethanol and dioxane exhibit markedly different liquefaction abilities, despite having similar total interaction energies with EHL.

The average number of hydrogen bonds formed between EHL and solvent molecules, as well as those formed within EHL itself, were calculated, see Fig. 5(a) and (b). Solvents with hydroxyl functional groups can form more hydrogen bonds with EHL. Water forms the most hydrogen bonds with EHL, averaging 41.87, followed by ethanol with an average of 22.08. In contrast, solvents containing ether or aldehyde oxygen atoms form significantly fewer hydrogen bonds with EHL, as seen in dioxane (9.15) and ethyl acetate (6.52). This is because the oxygen in ether or aldehyde groups is less accessible to EHL molecules for hydrogen bond formation compared to the oxygen in hydroxyl groups. Heptane does not form any hydrogen bond with EHL. The number of

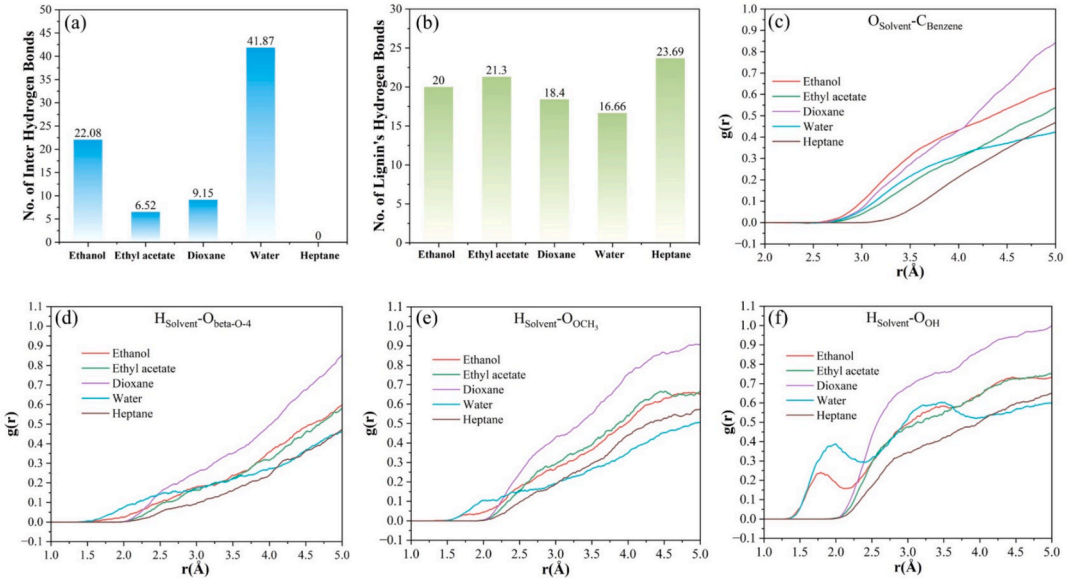

Fig. 5. (a) The number of hydrogen bonds between EHL molecules and different solvents, (b) the number of hydrogen bonds within EHL molecules, and the RDF curves between solvent molecules and EHL for (c-f) benzene rings, β-O-4, $–OCH_3$, and –OH groups.

hydrogen bonds formed within the EHL molecule may also influence their solubility, as shown in Fig. 5(b). In water, EHL forms a significant number of internal hydrogen bonds, averaging 16.66, likely due to the aggregation of EHL into spherical structures that limit the exposure of internal oxygen-containing functional groups to the solvent. The number of hydrogen bonds within EHL is 18.4 in dioxane and 20 in ethanol, respectively. Despite the fewer hydrogen bonds formed between dioxane and EHL, EHL can extend better in dioxane. In heptane, the number of internal hydrogen bonds within EHL is 23.69, which is the highest number among those in the five solvents, because no hydrogen bonds form between EHL and heptane, leading to significant EHL aggregation.

The radial distribution function (RDF) was analyzed to examine the distance and distribution density between solvent molecules and different functional groups in EHL. The RDF between the O atoms of the solvents (or C atoms for heptane) and the C atoms in the benzene rings of EHL plotted in Fig. 5(c) indicate that ethanol and dioxane molecules have a greater propensity to interact with the benzene rings. In Fig. 5 (d)–(f), the RDF analysis between the H atoms in the solvents and the O atoms in the OH, OCH_3, and β-O-4 functional groups of EHL indicate that water and ethanol molecules are more inclined to interact with the O atoms in EHL. Notably, within the 1.5–2 Å range surrounding the OH functional group in Fig. 5(f), both water and ethanol demonstrate a higher distribution density. In contrast, the distribution density around the oxygen atoms in the OCH_3 and β-O-4 functional groups is relatively weak, see Fig. 5(e). Thus, the hydrogen bonds between EHL and the solvents are mainly contributed by the OH functional group. Fig. 5(d) shows that water molecules have a greater propensity to interact with the O atom in the β-O-4 functional group. This behavior is likely associated with the molecular size of the solvents, where smaller molecule can access the O atoms more effectively.

3.3. The cAIMD simulation of the lignin dimer

Phenoxyethylbenzene was used as the lignin dimer model compound to investigate the cleavage of the β-O-4 bond in different solvents. Fig. 6 (a–b) demonstrates that the oxygen atom in the β-O-4 moiety can form hydrogen bond with ethanol and water molecules, whereas such interactions are not observed with ethyl acetate, dioxane, and heptane. During the cleavage of the β-O-4 bond, unstable EHL fragments are generated, with alkyl side chains undergoing dehydrogenation to form C=C double bonds, Fig. 6(c–g). This finding aligns with the observations in Fig. 2(f), where a higher concentration of monomer products containing C=C double bonds was detected. In solvents such as ethanol, ethyl acetate, dioxane, and heptane, the steric hindrance of molecular motion and the π-π conjugation of the benzene rings hinder the separation of the benzene rings within the dimer. Consequently, the hydrogen radical released from the alkyl side chains preferentially transfers to the 2-position carbon atom of the phenoxy radical. In contrast, within the aqueous solvent environment, Fig. 6(f), the reduced steric hindrance of the EHL fragments facilitates the separation of the benzene rings, allowing the oxygen atom of the phenoxy radical to be in closer proximity to the alkyl side chain. This proximity results in the preferential transfer of the hydrogen radical to the oxygen atom, leading to the formation of phenol.

The SG method was employed to calculate the free energy barriers for the cleavage of the β-O-4 chemical bonds and the self-hydrogenation step (Fig. 7(a–e)). It is noteworthy that the cleavage of the β-O-4 chemical bond is accompanied by hydrogen atom transfer, and these two processes are not entirely independent. With the β-O-4 chemical bond length as the collective variable (CV) and systematically varying the bond length, it is observed that the average constrained force on the system becomes zero when the bond length is approximately 1.4 Å. This point corresponds to the minimum free energy, indicating the most stable state of the dimer. As the bond length increases, the average

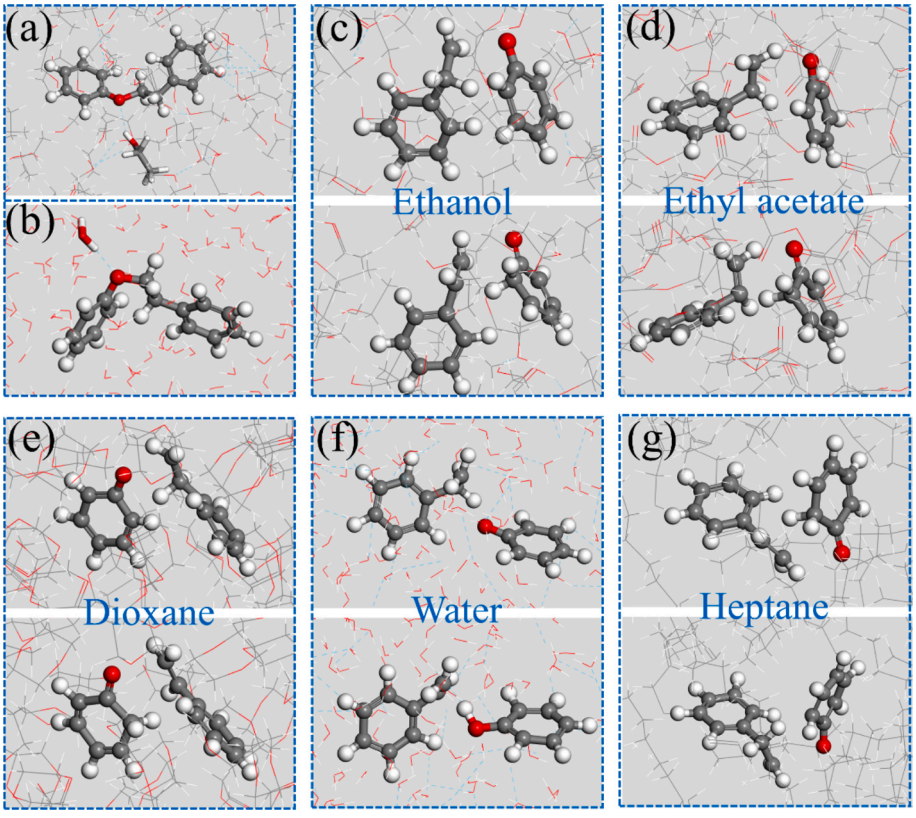

Fig. 6. The formation of hydrogen bonds between β-O-4 and (a) ethanol and (b) water molecules, and the hydrogen transfer process in (c) ethanol, (d) ethyl acetate, (e) dioxane, (f) water, and (g) heptane solvents.

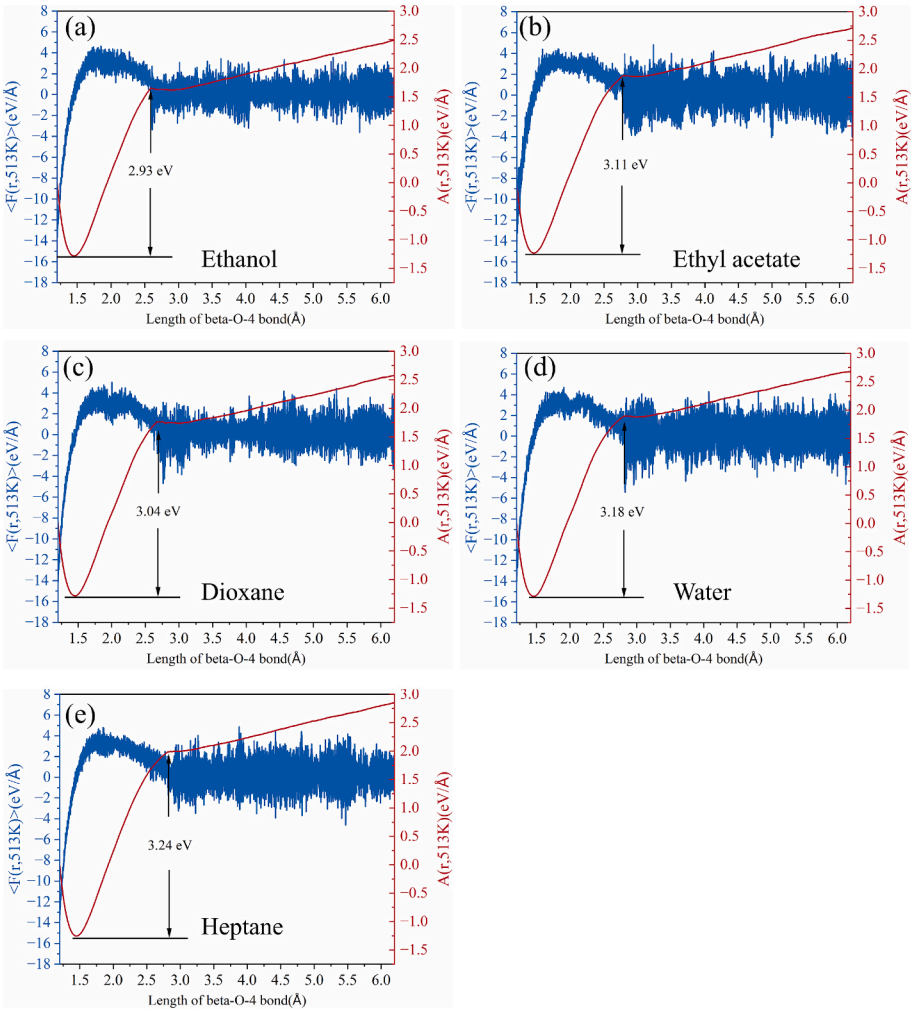

Fig. 7. (a–e) The β-O-4 bond cleavage barriers in the dimer model compound (phenoxyethylbenzene).

constrained force on the system first increases and then decreases until the bond length reaches 2.50–2.75 Å, where the average constrained force remains above zero, indicating that the β-O-4 chemical bond is completely broken with the H atom transfer completed. The free energy curve was derived by integrating the average constrained force, displaying a pronounced inflection point that corresponds to the complete cleavage of the chemical bond. The free energy difference between this inflection and the minimum points reflects the overall energy barrier for the β-O-4 bond cleavage and the associated hydrogen transfer in the dimer model compound. Within the bond length range of 2.75–6.0 Å, the free energy increases slowly due to the forced diffusion of the dimer fragments in the solvent. The β-O-4 bond cleavage barrier is the lowest in ethanol at 2.93 eV and the highest in heptane at 3.24 eV, consistent with the experimentally observed order of EHL monomer yields across different solvents. The lowest energy barrier in ethanol might be due to the stable hydrogen bonds formed between ethanol molecules and the oxygen atom in the β-O-4 chemical bond. Overall, the difference of the energy barriers of β-O-4 bond cleavage in all solvents is small, indicating that those solvents have a limited effect on β-O-4 chemical bond cleavage, which may explain the low monomer yields of EHL in all solvents observed experimentally.

4. Discussion

4.1. EHL dissolution

The solubility of EHL in different solvents varies significantly, with higher liquefaction degrees observed in dioxane and ethanol, and lower degrees in water and heptane. Understanding the underlying mechanisms of this variability is crucial for designing more effective EHL solvolysis strategies. MD simulations provide a microscopic insight into the stretching behavior of EHL molecules in various solvents. In dioxane, the EHL molecule extends into a linear chain, whereas in water and heptane, it aggregates into a spherical structure (Bogdan et al., 2023). These theoretical simulation results at the molecular level are consistent with the macroscopic solubility order observed in experiments.

The stretching behavior of EHL in different solvents is closely related to the interactions between the solvent and EHL, which can be divided into two types: van der Waals interactions and electrostatic interactions. The average van der Waals and electrostatic interaction energies between the solvent molecules and the EHL molecule were calculated, and the data were subsequently fitted to develop a model describing the relationship between these interactions and the liquefaction degree. The results indicate that both van der Waals interaction energy and electrostatic interaction energy contribute to the stretching of EHL, with van der Waals interactions having a more significant influence than that of electrostatic interactions. The RDF analysis between solvent molecules and the aromatic rings in EHL reveals that dioxane molecules, which exhibit stronger van der Waals interactions, are more likely to approach the aromatic rings. These van der Waals interactions can disrupt the π-π conjugation between the aromatic rings within EHL molecules, thereby facilitating the stretching of EHL (Sang et al., 2023; Zhang et al., 2017).

Although the total interaction energy between water and dioxane is very similar, EHL clearly aggregates in water. This is mainly because the

interaction between water and EHL is primarily electrostatic rather than van der Waals. Electrostatic interactions promote the solvolysis of EHL by forming hydrogen bonds between solvent molecules and EHL molecules, such as with the $–OCH_3$, –OH, and β-O-4 functional groups in EHL. These hydrogen bonds can effectively weaken the interaction within EHL molecules, thereby promoting the dissolution of EHL (Li et al., 2021; Sun et al., 2016).

4.2. EHL cleavage

The monomer yields of EHL in different solvents varies significantly. Except for dioxane, the order across different solvents is consistent with that of liquefaction degrees. In dioxane, the total monomer yield is 4.84 wt%, which is lower than that in ethanol, 6.54 wt%, and ethyl acetate, 5.15 wt%. The total monomer yield is influenced not only by the physical dissolution of EHL but also by the cleavage energy barrier of EHL. The traditional transition state (TS) method is inadequate for calculating the effect of solvents on the cleavage energy barrier of EHL. Therefore, the SG enhanced sampling method for the cAIMD simulation was employed. The results show that the cleavage of the β-O-4 bond involves a hydrogen transfer step, in which the alkyl side chain of the dimer undergoes dehydrogenation, resulting in the formation of a C=C double bond. In addition, ethanol as solvent interacts with the dimer compound by building stable hydrogen bonds with the ether oxygen. This interaction contributes to a reduction in the β-O-4 bond cleavage energy barrier, measured as 2.93 eV, thereby facilitating the generation of lignin monomers. Furthermore, ethanol serves as a capping agent, supplying ethyl groups to stabilize the free radicals present in EHL fragments, which consequently leads to the formation of ester products. (Huang et al., 2015b). In other solvents, i.e., ethyl acetate, dioxane, heptane, and water, the energy barriers for β-O-4 bond cleavage exhibit minimal variation, indicating that those solvents do not play a significant role in facilitating the cleavage of β-O-4 bonds.

The acceptor sites of hydrogen radicals vary depending on the solvent. In water, the oxygen atom in the phenoxy radical of the cleaved dimer acts as the acceptor site for hydrogen radicals, leading to the formation of phenol. This occurs because, after the β-O-4 bond cleavage, the oxygen atom in the phenoxy radical is positioned closer to the alkyl side chain, and the distance between the aromatic rings is relatively large. Consequently, the oxygen atom in the phenoxy radical serves as the acceptor for hydrogen radicals rather than the carbon atoms within the aromatic ring. However, in solvents such as ethanol, ethyl acetate, dioxane, and heptane, the carbon atom in the phenoxy radical is the acceptor site for hydrogen radicals. This is possibly due to the increased spatial hindrance of molecular motion, making it more difficult for the aromatic rings within the dimer to separate. Thus, the hydrogen radicals removed from the alkyl side chain are more likely to approach the aromatic ring. Relevant literature also indicates that the carbon atom of the phenoxy radical is capable of accepting hydrogen radicals (Chen et al., 2018).

5. Conclusions

The solvolysis of EHL was investigated in fuel-compatible solvents, such as ethanol, ethyl acetate, dioxane, and heptane, as well as in the reference solvent, water. The results show that the liquefaction degree was highest in dioxane, while the monomer yield was highest in ethanol. In contrast, both the liquefaction degree and monomer yield were low in water and heptane. By fitting the relationship between the liquefaction degree and the van der Waals and electrostatic interaction energies between the solvent and EHL, it was found that both interaction energies contribute to the EHL solvolysis, with van der Waals interactions having a greater influence than the electrostatic interactions. Van der Waals forces weaken the π-π conjugation between aromatic rings within EHL molecules, while electrostatic forces promote EHL depolymerization through forming hydrogen bonds. The energy barrier for β-O-4 bond cleavage was lowest in ethanol, due to the stable hydrogen bonds formed between ethanol molecules and the ether oxygen in the dimer model compound. During the cleavage of β-O-4 bonds, hydrogen transfer occurs simultaneously to stabilize the free radicals produced in the EHL.

The solvolysis of EHL in solvent involves both physical dissolution and chemical depolymerization steps. Although these processes are interconnected, the microscopic mechanisms of solvolysis can be investigated separately. The physical dissolution process is mainly driven by the extension of EHL molecules within the solvent, occurring in the absence of chemical reactions. In contrast, chemical depolymerization involves the cleavage of specific bonds between lignin units within EHL molecules, such as the predominant β-O-4 linkages.

CRediT authorship contribution statement

Gen Li: Writing – original draft, Validation, Methodology, Investigation, Data curation, Conceptualization. **Yushuai Sang:** Validation, Methodology, Investigation. **Xiang Li:** Validation, Resources, Methodology, Investigation. **Hong Chen:** Validation, Supervision, Resources, Methodology. **Yongdan Li:** Writing – review & editing, Validation, Supervision, Resources, Methodology, Funding acquisition, Conceptualization.

Declaration of competing interest

The authors declare that they have no known competing financial interests or personal relationships that could have appeared to influence the work reported in this paper.

Acknowledgements

This work was funded by the European Union's Horizon 2020 research and innovation program, (BUILDING A LOW-CARBON, CLIMATE RESILIENT FUTURE: SECURE, CLEAN AND EFFICIENT ENERGY) under Grant Agreement No 101006744. The content presented in this document represents the views of the authors, and the European Commission has no liability in respect of the content. G. Li would like to express his gratitude to both the China Scholarship Council (202208320030) and the EU-101006744 project.

Data availability

Data will be made available on request.

References

Bai, Y., Cui, K., Sang, Y., Wu, K., Yan, F., Mai, F., Ma, Z., Wen, Z., Chen, H., Chen, M., Li, Y., 2019. Catalytic depolymerization of a lignin-rich corncob residue into aromatics in supercritical ethanol over an alumina-supported NiMo alloy catalyst. Energy Fuels 33, 8657–8665.

Barta, K., Matson, T.D., Fettig, M.L., Scott, S.L., Iretskii, A.V., Ford, P.C., 2010. Catalytic disassembly of an organosolv lignin via hydrogen transfer from supercritical methanol. Green Chem. 12, 1640–1647.

Bogdan, T.V., Bobrova, N.A., Koklin, A.E., Mishanin, I.I., Odintsova, E.G., Antipova, M.L., Petrenko, V.E., Bogdan, V.I., 2023. Structure of aqueous solutions of lignin treated by sub- and supercritical water: Experiment and simulation. J. Mol. Liq. 383.

Carter, E.A., Ciccotti, G., Hynes, J.T., Kapral, R., 1989. Constrained reaction coordinate dynamics for the simulation of rare events. Chem. Phys. Lett. 156, 472–477.

Chen, H., He, Y., Pfefferle, L.D., Pu, W., Wu, Y., Qi, S., 2018. Phenol catalytic hydrogenation over palladium nanoparticles supported on metal-organic frameworks in the aqueous phase. ChemCatChem 10, 2558–2570.

Chen, J., Wang, C., Shang, W., Bai, Y., Wu, X., 2023. Study on the mechanisms of hydrogen production from alkali lignin gasification in supercritical water by ReaxFF molecular dynamics simulation. Energy 278.

Fang, Y., Yin, L., Yang, H., Gong, X., Chen, Y., Chen, H., 2021. Catalytic mechanisms of potassium salts on pyrolysis of β-O-4 type lignin model polymer based on DFT study. Proc. Combust. Inst. 38, 3969–3976.

Fei, Z., Chen, D., Hensen, E.J.M., Li, Y., Jagadeesh, R.V., 2023. Catalytic valorization of lignocellulose and its derived feedstocks into fuels and chemicals. Catal. Today 408, 1.

Grimme, S., Antony, J., Ehrlich, S., Krieg, H., 2010. A consistent and accurate ab initio parametrization of density functional dispersion correction (DFT-D) for the 94 elements H-Pu. J. Chem. Phys. 132.
Hu, H., Yun, R.H., Hermans, J., 2002. Reversibility of free energy simulations: Slow growth may have a unique advantage. (with a note on use of ewald summation). Mol. Simul. 28, 67–80.
Huang, X., Atay, C., Koránya, T.I., Boot, M.D., Hensen, E.J.M., 2015a. Role of Cu-Mg-Al mixed oxide catalysts in lignin depolymerization in supercritical ethanol. ACS Catal. 5, 7359–7370.
Huang, X., Koránya, T.I., Boot, M.D., Hensen, E.J.M., 2014. Catalytic depolymerization of lignin in supercritical ethanol. ChemSusChem 7, 2276–2288.
Huang, X., Koránya, T.I., Boot, M.D., Hensen, E.J.M., 2015b. Ethanol as capping agent and formaldehyde scavenger for efficient depolymerization of lignin to aromatics. Green Chem. 17, 4941–4950.
Jiang, X., Lu, Q., Hu, B., Chen, D., Liu, J., Dong, C., 2019. Influence of inherent alkali metal chlorides on pyrolysis mechanism of a lignin model dimer based on DFT study. J. Therm. Anal. Calorim. 137, 151–160.
Kouris, P.D., van Osch, D.J.G.P., Cremers, G.J.W., Boot, M.D., Hensen, E.J.M., 2020. Mild thermolytic solvolysis of technical lignins in polar organic solvents to a crude lignin oil. Sustain. Energ. Fuels 4, 6212–6226.
Li, C., Zhao, X., Wang, A., Huber, G.W., Zhang, T., 2015. Catalytic transformation of lignin for the production of chemicals and fuels. Chem. Rev. 115, 11559–11624.
Li, Q., Dong, Y., Hammond, K.D., Wan, C., 2021. Revealing the role of hydrogen bonding interactions and supramolecular complexes in lignin dissolution by deep eutectic solvents. J. Mol. Liq. 344.
Ma, R., Hao, W., Ma, X., Tian, Y., Li, Y., 2014. Catalytic ethanolysis of kraft lignin into high-value small-molecular chemicals over a nanostructured α-molybdenum carbide catalyst. Angew. Chem. Int. Ed. 53, 7310–7315.
Ma, Y., Sang, Y., Wu, K., Liu, Q., Chen, H., Li, Y., 2023. Selective production of 2-(tert-butyl)-3-methylphenol from depolymerization of enzymatic hydrolysis lignin with MoS2 catalyst. Catal. Today 408, 194–203.
Mai, F., Wen, Z., Bai, Y., Ma, Z., Cui, K., Wu, K., Yan, F., Chen, H., Li, Y., 2019. Selective conversion of enzymatic hydrolysis lignin into alkylphenols in supercritical ethanol over a WO3/γ-Al2O3 catalyst. Ind. Eng. Chem. Res. 58, 10255–10263.
Mariano Colombari, F., Marcos Nascimento, V., Liu, Y.L., de Morais Rocha, G.J., Driemeier, C., 2022. Density functional theory with implicit solvents for accurate estimation of aqueous and organic solvation free energies of lignin fragments. ACS Sustain. Chem. Eng. 10, 10870–10878.
Martyna, G.J., Klein, M.L., Tuckerman, M., 1992. Nosé-Hoover chains: The canonical ensemble via continuous dynamics. J. Chem. Phys. 97, 2635–2643.
Menezes, F.F., Nascimento, V.M., Gomes, G.R., Rocha, G.J.M., Strauss, M., Junqueira, T. L., Driemeier, C., 2023. Depolymerization of enzymatic hydrolysis lignin: Review of technologies and opportunities for research. Fuel 342.
Nielsen, J.B., Jensen, A., Madsen, L.R., Larsen, F.H., Felby, C., Jensen, A.D., 2017. Noncatalytic direct liquefaction of biorefinery lignin by ethanol. Energy Fuels 31, 7223–7233.
Obydenkova, S.V., Kouris, P.D., Hensen, E.J.M., Smeulders, D.M.J., van der Meer, Y., Boot, M.D., 2019. Industrial lignin from 2g biorefineries-assessment of availability and pricing strategies. Bioresour. Technol. 291.
Pang, Y., Zhu, X., Li, N., Wang, Z., 2023. Investigation on reaction mechanism for CO2 gasification of softwood lignin by ReaxFF MD method. Energy 267.
Perdew, J.P., Burke, K., Ernzerhof, M., 1997. Generalized gradient approximation made simple. Phys. Rev. Lett. 78, 1396.
Ponnuchamy, V., Sandak, J., Sandak, A., 2021. Revealing of supercritical water gasification process of lignin by reactive force field molecular dynamics simulations. Processes 9, 714.
Sang, Y., Chen, M., Yan, F., Wu, K., Bai, Y., Liu, Q., Chen, H., Li, Y., 2020. Catalytic depolymerization of enzymatic hydrolysis lignin into monomers over an unsupported nickel catalyst in supercritical ethanol. Ind. Eng. Chem. Res. 59, 7466–7474.
Sang, Y., Li, G., Li, X., Gong, H., Yang, M., Savary, D., Fei, Z., Dyson, P.J., Chen, H., Li, Y., 2024. A synergistic approach for lignin biofuel production: Integrating non-catalytic solvolysis with catalytic product upgrading. Chem. Eng. J. 495.
Sang, Y., Ma, Y., Li, G., Cui, K., Yang, M., Chen, H., Li, Y., 2023. Enzymatic hydrolysis lignin dissolution and low-temperature solvolysis in ethylene glycol. Chem. Eng. J. 463.
Sang, Y., Wu, K., Liu, Q., Bai, Y., Chen, H., Li, Y., 2021. Catalytic ethanolysis of enzymatic hydrolysis lignin over an unsupported nickel catalyst: The effect of reaction conditions. Energy Fuels 35, 519–528.
Shankar, U., Gogoi, R., Sethi, S.K., Verma, A., 2022. Introduction to materials studio software for the atomistic-scale simulations. In: Verma, A., Mavinkere Rangappa, S., Ogata, S., Siengchin, S. (Eds.), Forcefields for Atomistic-Scale Simulations: Materials and Applications. Springer Nature Singapore, Singapore, pp. 299–313.
Shen, Q., Fu, Z., Li, R., Wu, Y., 2021. A study on the pyrolysis mechanism of a β-O-4 lignin dimer model compound using DFT combined with Py-GC/MS. J. Therm. Anal. Calorim. 146, 1751–1761.
Shen, X., Zhang, C., Han, B., Wang, F., 2022. Catalytic self-transfer hydrogenolysis of lignin with endogenous hydrogen: Road to the carbon-neutral future. Chem. Soc. Rev. 51, 1608–1628.
Sprik, M., Ciccotti, G., 1998. Free energy from constrained molecular dynamics. J. Chem. Phys. 109, 7737–7744.
Sumer, Z., Van Lehn, R.C., 2022. Data-centric development of lignin structure-solubility relationships in deep eutectic solvents using molecular simulations. ACS Sustain. Chem. Eng. 10, 10144–10156.
Sun, J., Dutta, T., Parthasarathi, R., Kim, K.H., Tolic, N., Chu, R.K., Isern, N.G., Cort, J.R., Simmons, B.A., Singh, S., 2016. Rapid room temperature solubilization and depolymerization of polymeric lignin at high loadings. Green Chem. 18, 6012–6020.
VandeVondele, J., Krack, M., Mohamed, F., Parrinello, M., Chassaing, T., Hutter, J., 2005. Quickstep: Fast and accurate density functional calculations using a mixed gaussian and plane waves approach. Comput. Phys. Commun. 167, 103–128.
Wang, J., Qian, Y., Li, L., Qiu, X., 2020. Atomic force microscopy and molecular dynamics simulations for study of lignin solution self-assembly mechanisms in organic-aqueous solvent mixtures. ChemSusChem 13, 4420–4427.
Wu, K., Sang, Y., Kasipandi, S., Ma, Y., Jiao, H., Liu, Q., Chen, H., Li, Y., 2023. Catalytic roles of Mo-based sites on MoS2 for ethanolysis of enzymatic hydrolysis lignin into aromatic monomers. Catal. Today 408, 211–222.
Wu, X., Lian, H., Li, X., Xiao, J., 2023. The mechanism of self-assembly of lignin in deep eutectic solvent based on sulfamic acid and urea through molecular dynamics simulation. Int. J. Biol. Macromol. 253.
Yan, N., Zhao, C., Dyson, P.J., Wang, C., Liu, L., Kou, Y., 2008. Selective degradation of wood lignin over noble-metal catalysts in a two-step process. ChemSusChem 1, 626–629.
Yang See, J., Song, S., Xiao, Y., Trang Pham, T., Zhao, Y., Lapkin, A., Yan, N., 2021. Transformation of corn lignin into sun cream ingredients. ChemSusChem 14, 1586–1594.
Zhan, W., Peng, D., Li, K., Liang, Z., Bu, Y., Sun, Z., Jiang, C., Zhang, J., 2024. Effect of Fe and its oxides on steam gasification mechanism of lignin using ReaxFF molecular dynamics simulations. J. Energy Inst. 114.
Zhang, T., Li, X., Guo, L., Guo, X., 2019. Reaction mechanisms in pyrolysis of hardwood, softwood, and kraft lignin revealed by ReaxFF MD simulations. Energy Fuels 33, 11210–11225.
Zhang, Y., He, H., Dong, K., Fan, M., Zhang, S., 2017. A DFT study on lignin dissolution in imidazolium-based ionic liquids. RSC Adv. 7, 12670–12681.